# Accepted Manuscript

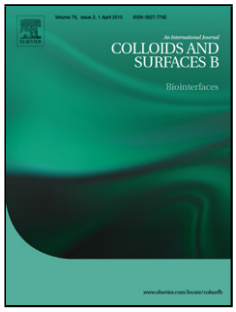


Title: Modified bacterial cellulose scaffolds for localized doxorubicin release in human colorectal HT-29 cells

Author: Maximiliano L. Cacidedo Ignacio E. León Jimena S. Gonzalez Luismar M. Porto Vera A. Alvarez Guillermo R. Castro

PII: S0927-7765(16)30006-6
DOI: http://dx.doi.org/doi:10.1016/j.colsurfb.2016.01.007
Reference: COLSUB 7584

To appear in: *Colloids and Surfaces B: Biointerfaces*

Received date: 13-9-2015
Revised date: 6-12-2015
Accepted date: 3-1-2016

Please cite this article as: Maximiliano L.Cacidedo, Ignacio E.León, Jimena S.Gonzalez, Luismar M.Porto, Vera A.Alvarez, Guillermo R.Castro, Modified bacterial cellulose scaffolds for localized doxorubicin release in human colorectal HT-29 cells, Colloids and Surfaces B: Biointerfaces http://dx.doi.org/10.1016/j.colsurfb.2016.01.007

# Modified bacterial cellulose scaffolds for localized doxorubicin release in human colorectal HT-29 cells

Maximiliano L. Cacicedo[1], Ignacio E. León[2], Jimena S. Gonzalez[3], Luismar M. Porto[4], Vera A. Alvarez[3] and Guillermo R. Castro[1]

[1] Nanobiomaterials Laboratory, Institute of Applied Biotechnology (CINDEFI, UNLP-CONICET-CCT La Plata), Department of Chemistry, School of Sciences, Universidad Nacional de La Plata, Calle 47 y115, CP 1900 La Plata, Argentina.

[2] Chemical Inorganic Center (CEQUINOR, UNLP, CONICET), School of Sciences, Universidad Nacional de La Plata (UNLP), Calle 47 y 115, (1900) La Plata, Argentina

[3] CoMP (Composite Materials Group), Research Institute of Material Science and Technology (INTEMA), Engineering School, National University of Mar del Plata, Solis 7575, (B7608FDQ) Mar del Plata, Argentina

[4] Integrated Technologies Laboratory (InteLAB), CTC/EQA, Universidad Federal de Santa Catarina, Florianopolis, Brazil.

Corresponding Author: Guillermo R. Castro
E-mail: grcastro@gmail.com
Phone: ++54.221.4833794 ext. 132 (Office)

**Graphical abstract**

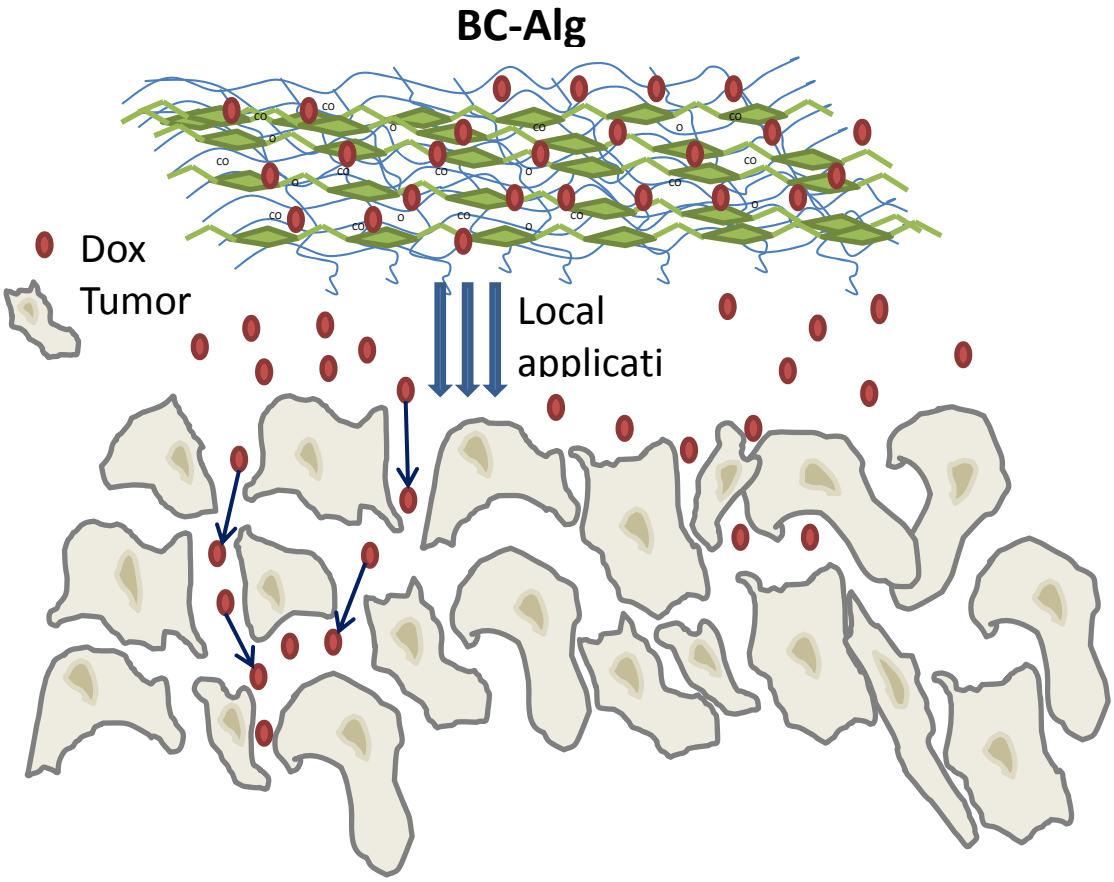

## Highlights

- *In-situ* modification of bacterial cellulose membranes with alginate was performed.
- The hybrid bacterial cellulose-alginate membranes are able to control release doxorubicin.
- FTIR, XRD, TGA and SEM of bacterial cellulose-alginate scaffolds showed strong interconnected hybrid network with enhanced hydrophilicity.
- The bacterial cellulose-alginate matrix was able to incorporate from 3.7 μg/g to 11.0 μg/g doxorubicin/matrix range with linear responses.
- Brunauer–Emmett–Teller and Barrett–Joyner–Halenda analyses of the bacterial cellulose-alginate scaffolds showed an increase of the surface area in about 84% and the rise of pore volume for more than 200% compared to BC films.
- The bacterial cellulose-alginate containing doxorubicin showed high efficiency on killing HT-29 human colorectal adenocarcinoma cells compared to free doxorubicin in the same range concentrations.

## Abstract

Bacterial cellulose (BC) films modified by the *in situ* method with the addition of alginate (Alg) during the microbial cultivation of *Gluconacetobacter hansenii* under static conditions increased the loading of doxorubicin by at least three times. Biophysical analysis of BC-Alg films by scanning electron microscopy, thermogravimetry, X-ray diffraction and FTIR showed a highly homogeneous interpenetrated network scaffold without changes in the BC crystalline structure but with an increased amorphous phase. The main molecular interactions determined by FTIR between both biopolymers clearly suggest high compatibility. These results indicate that alginate plays a key role in the biophysical properties of the hybrid BC matrix. BC-Alg scaffold analysis by nitrogen adsorption isotherms revealed by the Brunauer–Emmett–Teller (BET) method an increase in surface area of about 84% and in pore volume of more than 200%. The Barrett–Joyner–Halenda (BJH) model also showed an increase of about 25% in the pore size compared to the BC film.

Loading BC-Alg scaffolds with different amounts of doxorubicin decreased the cell viability of HT-29

human colorectal adenocarcinoma cell line compared to the free Dox from around 95% to 53% after 24 h and from 63% to 37% after 48 h. Dox kinetic release from the BC-Alg nanocomposite displayed hyperbolic curves related to the different amounts of drug payload and was stable for at least 14 days. The results of the BC-Alg nanocomposites show a promissory potential for anticancer therapies of solid tumors.

**Keywords:** bacterial cellulose, alginate, drug delivery, nanocomposite, doxorubicin, cancer therapy, human colorectal HT-29 cells

## 1. Introduction

Cancer, one of the leading causes of death worldwide, accounted for 8.2 million diseases in 2012 [1]. Typically, cancer arises from a normal cell that undergoes a transformation into an abnormal cell, and consequently a malignant tumor develops. Although the choice of drug chemotherapy depends on the type of cancer pathology, tumor stage and patient characteristics and tolerance, the surgical resection of the tumor is the preferred treatment once cancer has been diagnosed [2]. Nevertheless, chemo- and/or radiotherapies are always involved in most types of cancer diseases. In the case of chemotherapy, the drugs always show serious limitations severely affecting the patient's health, recovery and quality of life. These limitations may be due to poor drug solubility, high toxicity, immune suppression, red blood cell and stem cell depletion, high dosage and nonspecific action [3]. Additionally, by intravenous (*iv*) drug administration, it is very difficult to keep medicine concentrations surrounding the tumor microenvironment within the therapeutic window. Besides, ~~the~~ chemo-resistance to standard treatments develops in nearly all patients [4]. Therefore, in the chemotherapeutic regimens, high *iv* drug doses are given with the consequent adverse side effects and drug accumulation on nontargeted tissues [5]. Among them, doxorubicin (Dox), a member of the anthracycline family, is extensively used in anticancer treatments but it causes very well-described undesirable side effects such as cardiotoxicity, depletion of red blood cells (anemia), hair loss, stomach pain and others [6].

The ability of anticancer drugs to reach the appropriate anatomic region of the body where the tumor is located is always relevant and has been the subject of intense research during the last 10 years. Different new surgical possibilities, pharmaceutical molecules, drug delivery techniques and devices, among others, play a major role in the development of novel and personalized cancer therapies. Particularly, localized delivery of chemotherapeutic agents may help to achieve better results than those of systemic chemotherapy. In this sense, local application of a drug delivery device within a specific zone where cancer cells are proliferating will generate a major exposure of those cells to the chemotherapeutic drugs and it may: (i) decrease toxic adverse effects by using lower drug doses; (ii) decrease tumor volume more efficiently, increasing surgeons' possibility to succeed in total tumor resection; (iii) enhance the effect of regular chemotherapy in the case of nonviable surgery. Local drug delivery is a recent alternative for the therapy of some solid tumors that reduce the chemotherapeutic toxicity and can provide better regimens using clinically approved drugs [7]. Also, anticancer therapies with local drug delivery could be used in those cases where surgery cannot be an alternative or effective without compromising healthy tissues or physiologically functional organs. Another option might be the application of the films in order to reduce tumor volume before surgery or as adjuvant targeted therapy to prevent tumor recurrence after surgery [8,9].

Matrices composed of biopolymer blends are promising candidates for the development of local drug delivery systems. These polymers have several advantages, such as synthesis methods based on *Green chemistry*, availability in large quantities, and nontoxic properties as they are listed in the

GRAS (generally recognized as safe, FDA, US) category, are renewable, easy to handle, biodegradable, commercially available and generally of low cost. Among them, alginates are GRAS polymers extensively studied for many pharmaceutical and food applications [10]. Alginate is a biopolymer composed of guluronic and mannuronic acids produced by algae and some bacteria. Alginate is able to cross-link in the presence of polyvalent cations forming stable gels commonly named "egg-box" structures. Calcium is the typical cross-linker for biomedical and food industry applications because of its lack of toxicity. Previous results in our laboratory demonstrated the potential use of alginates in the synthesis of drug delivery devices [11–13].

Lately, bacterial cellulose (BC) has been intensively studied for many industrial applications including the biomedical field, such as tissue engineering and drug delivery [14]. BC is an extracellular polysaccharide detected in gram-positive and especially in gram-negative bacteria at the air/culture media interface. The most efficient cellulose producers are members of the acetic acid bacteria, and particularly *Gluconacetobacter hansenii* has been extensively used as a BC producer model. BC is produced in nanofibrils composed of β-1→4 linkages of glucose units stabilized by inter- and intrachain hydrogen bridges. In static microbial cultures, the BC nanofibrillar structure is roughly 10 nm thick and 50 nm wide extremely pure cellulose network showing high water content (more than 90%), high mechanical strength and well-defined biocompatibility [14]. Native BC presents some properties that contribute to making it a good biomaterial to be used as a matrix for localized drug delivery. Such properties involve the stability of the material at high temperatures, facilitating its sterilization by autoclaving [15]. Its flexibility and porosity, similar to that of collagen, might be one of the reasons for its well-tolerated biocompatibility [14]. Besides, BC can be purified reaching endotoxin values of <20 endotoxin units/device approved by the FDA for implants [16]. However, plain BC films are not able to entrap, keep and control the release of Dox. In order to provide the properties of drug controlled release, recently a novel strategy for the *ex situ* modification of native bacterial cellulose films was reported [17]. The BC scaffold was modified by an *ex situ* method with the synthesis of $CaCO_3$-carragenaan microparticles containing Dox on the film surface. The $CaCO_3$ microparticles containing Dox were responsible for the sustained release of the drug and stable on shelf for more than one year [17]. Alternatively, BC films could be modified by the *in situ* method consisting in the addition of molecules during the initial stages of bacterial fermentation. When BC was reinforced by *in situ* modification using polymers, such as gelatin, collagen and chitosan for biomedical purposes, novel biophysical film properties were found [18]. In this sense, the addition of negatively charged polymers such as alginates to bacterial cultures during BC synthesis could enhance the interaction between the hybrid films and Dox, as previously reported for the pectin-Dox model [19]. Recently, native or chemically modified BC-alginate composites were found to be versatile systems for mammalian eukaryotic cell cultivation because of the ductility and functionally of nanocellulose-alginate networks [20–22]. Also, BC and alginate were mixed by an ex situ method with silver sulfadiazine payload [23]. Additionally, the synthesis of BC nanocomposite in the presence of

low sodium alginate concentration (0.04%) by *A. xylinum* was studied [24].

In the present study, nanocomposite bacterial cellulose films modified *in situ* by the addition of alginate during the static cultivation of *Gluconacetobacter hansenii* were produced to formulate scaffolds containing doxorubicin for cancer treatment. The nanocomposite films were purified and characterized by thermogravimetry (TGA), X-ray diffraction (XRD), infrared spectroscopy (FTIR), optical, fluorescence and scanning electron microscopy (SEM), BET-BJH (Brunauer–Emmett–Teller and the Barrett–Joyner–Halenda) methods. In addition, Dox loading and drug kinetic release are reported. Finally, the effect of Dox release from the BC-alginate nanocomposite films was tested on the human colorectal adenocarcinoma cell line (HT-29) in order to test the therapeutic effect in comparison to the direct exposure to Dox.

## 2. Materials and Methods

### 2.1. Chemicals and media

Sodium alginate was purchased from Monsanto Co. Doxorubicin (Dox, MW 579.98) was kindly supplied by LKM pharmaceuticals (Argentina). All other reagents used were of analytical or microbiological grade and purchased from Sigma-Aldrich (St. Louis, MO) or Merck (Darmstadt, Germany) except as otherwise indicated.

Dox was quantified by spectrofluorimetry (Perkin Elmer LS 50B, Japan) using $\lambda_{exc}$ 476 nm and $\lambda_{em}$ 588 nm with appropriate calibration curves.

Cell culture materials were purchased from Corning (Princeton, NJ, USA), Dulbecco´ s Modified Eagles Medium (DMEM), TrypLE$^{TM}$ from Gibco (Gaithersburg, MD, USA), and fetal bovine serum (FBS) from Internegocios SA (Argentina). All other chemicals were from Sigma Chemical Co. (ST. Louis, MO).

### 2.2. Microbial cellulose production with sodium alginate addition

Bacterial cellulose was synthesized by *Gluconacetobacter hansenii* (ATCC 23769) grown statically in the following medium, in g $l^{-1}$: 25.0 manitol, 5.0 yeast extract, 3.0 peptone. Sodium alginate was added at concentrations of 1.0%. The pH media was adjusted to 6.5 with 0.1M NaOH solution before sterilization. The culture was kept statically in 96-well plates at 27°C for 14 days.

### 2.3. Microbial cellulose purification

Native cellulose and hybrid cellulose films were collected from the plates for the purification process and washed three times with a 70% ethanol solution for 60 min. Later, the purification was performed using 70% ethanol/0.1 N NaOH solution for 24 h at 30ºC. After that, repetitive washes with 70% ethanol were done until neutral pH was reached. Finally, the films were exposed to a solution of 70% ethanol/ 0.5M $CaCl_2$, in order to achieve ionic gelation of the alginate remaining inside the cellulose.

**2.4. Biomaterial characterization**

**2.4.1. Thermogravimetric analysis (TGA)**

Dynamic thermogravimetric measurements of native and hybrid bacterial cellulose membranes were performed by using a Shimadzu TGA-50 instrument. Tests were run from 20ºC to 900ºC at a heating rate of 10ºC/min under $N_2$ atmosphere.

**2.4.2. X-ray diffraction (XRD)**

XRD patterns of cellulose film samples were collected in reflection mode on a glass substrate. The measurement was performed with an Analytical Expert instrument using Cu-$K_\alpha$ radiation ($\lambda$= 1.54 Å) from 2$\theta$= 10 to 70º in continuous mode with 0.07º step size. The results were analyzed using Origin software.

**2.4.3. Fourier transform infrared spectroscopy (FTIR)**

The FTIR spectra of the lyophilized samples were recorded in a spectrometer (Thermo Scientific Nicolet, 6700 model, CT, USA) coupled with an ATR (attenuated total reflectance) accessory for all measurements. A number of 32 scans were performed for each sample in the 600 to 4,000 $cm^{-1}$ range and resolution of 4 $cm^{-1}$.

**2.4.4. Scanning electron microscopy (SEM)**

Samples were firstly dried by the critic point technique. After that, the surface was sputtered with gold using a metalizer (Balzers SCD 030), obtaining a layer thickness between 15 and 20 nm. Film surfaces and morphologies were observed by SEM (Philips SEM 505 model, Rochester, NY, USA), and the images were processed by an image digitizer program (Soft Imaging System ADDA II).

**2.4.5. Roughness analysis**

SEM images were analyzed by ImageJ software (NIH, USA). The roughness of the surface was reflected by the standard variation of the gray values of all the pixels on the image. First, the SEM image files were opened by the software and converted to an 8-bit image. Then, all the pixels on the image were selected and statistically measured by a computer equipped with the software. The less the standard variation value is, the smoother the surface is. Histograms of SEM images at 1000x magnification were performed.

**2.4.6. Optical and fluorescence microscopy**

Drug loaded hybrid films were placed on 48-well plates with the same media and conditions as those of cell culture assays. Also, free Dox was used in the same concentration range used for cell cultures. After 24 and 48 h a sample was taken from each well and analyzed by microscopy. Optical and fluorescence microscopy was carried out in Leica DM 2500 microscope (Wetzlar, Germany) equipped with filter N2.1 for excitation in the green zone. Excitation filter BP: 515-560 nm, monochromatic mirror: 580nm, suppressor filter LP: 590nm.

**2.4.7. Nitrogen adsorption isotherms (BET)**

Nitrogen adsorption–desorption at 77 K at a bath temperature of −195.8 ・C was carried out for dry native and hybrid cellulose films. The surface area, pore volume and pore size of both membranes

were calculated with Micromeritics ASAP 2020 V3.00 software using the Brunauer–Emmett–Teller (BET) equation and the Barrett–Joyner–Halenda (BJH) method.

**2.5. Doxorubicin loading studies**

BC systems were immersed in Dox solutions with 3.7 μmols to 11.0 μmols in ethanol 80% solution and stirred at 230 rpm, at 25 °C for 20 h. The pH was measured before and after the procedure; no change was observed (pH= 7.0). The membranes were taken out from the vials and residual Dox was spectrofluorometrically assayed in the supernatants [17]. Membranes were washed one time in ethanol 80% and later in physiologic solution for 10 min. The loading efficiency was evaluated as follows:

$$\text{Dox incorporation} = \frac{(Dox_I - Dox_S)}{W_{BC}}$$

Where $Dox_I$ are the μmols of doxorubicin at time zero, $Dox_S$ are the μmols of doxorubicin in the supernatant and $W_{BC}$ is the mass of the BC film (grams).

Control assays without membranes were performed. Neither Dox degradation, nor fluorescence maximum shift or intensity decrease were observed after the encapsulation procedure.

**2.6. *In vitro* drug release studies**

BC membranes were placed in 1.5 ml physiologic solution on 2.0-ml plastic vials and thermostated at 37 °C. Samples of 500 μl were withdrawn and refilled with an equal volume of fresh buffer at defined intervals. Dox concentration was determined by fluorescence as mentioned before. Release experiments were performed two times in quadruplicate for each concentration.

**2.7. Cell line and growth conditions**

HT-29 human colon adenocarcinoma cells (HTB-38™) were grown in DMEM containing 10% FBS, 100 U/ml penicillin and 100 μg/ml streptomycin at 37 °C in 5% $CO_2$ atmosphere. Cells were seeded in a 75 $cm^2$ flask and when 70%–80% of confluence was reached, cells were subcultured using 1mL of TrypLE™ per 25 $cm^2$ flask. For the experiments, cells were grown in multiwell plates. When cells reached the desired confluence, the monolayers were washed with DMEM and were incubated under different conditions according to the experiments.

**2.8. Cell viability: Crystal violet assay**

A mitogenic bioassay was carried out as described previously with some modifications [25]. Briefly, cells were grown in 48-well plates. For the experiments, 3.0 x$10^4$ cells/ml were grown for 24 h at 37 °C. Then, the monolayers were incubated for 24 and 48 h with different concentrations (100–200 μM) of free doxorubicin or with the different BC matrices with and without drug (control) for the viability assays. After this treatment, the monolayers were washed with PBS and fixed with 5.0% glutaraldehyde / PBS at room temperature for 10 min. After that, the cells were stained with 0.5% crystal violet / 25% methanol for 10 min. Then, the dye solution was discarded, and the plate was

washed with water and dried. The dye taken up by the cells was extracted using 500 µL/well 100 mM glycine/HCl buffer (pH 3.0) / 30% methanol and transferred to test tubes. After a convenient sample dilution, the absorbance was read at 540 nm. It was previously shown that under these conditions, the colorimetric bioassay strongly correlated with cell proliferation measured by cell counting in Neubauer chamber [26].

## 3. Results and Discussion

### 3.1. Biomaterial characterization

The thermal properties of native bacterial cellulose (BC), alginate (Alg) and bacterial cellulose-alginate (BC-Alg) films were investigated by thermogravimetric analysis (**Figure 1A)**. Thermogravimetry (TGA) of unmodified bacterial cellulose displayed two decomposition steps in the curve. Meanwhile, the weight loss profiles for Alg and BC-Alg were different since they showed a three-step curve. The first step was attributed to unbound water content, observed in the temperature range between 30 °C and 120 °C. At 180 °C the percentage of weight loss was around 7% for BC, 18% for Alg and 20% for BC-Alg. The results show higher water content for the hybrid matrix as compared to BC membrane because of the alginate high hydrophilicity. It is generally accepted that water acts as plasticizer in polymeric matrices [27]. The increase of hydrophilicity in the BC film is advantageous since it could be related to the drug loading rise of water-soluble molecules such as doxorubicin.

The second step of BC and BC-Alg samples in the TGA curves was attributed to thermal decomposition of the biomaterials (**Figure 1A)**. The decomposition temperature of BC to BC-Alg curves shifted down from 350 °C to 300 °C, respectively (**Figure 1A)**. Particularly, the weight loss was about 30% in the 200–400 ºC range of BC-Alg films, half of the BC film mass loss in the same temperature range (**Table I**). The high thermal stability of BC-Alg hybrid films compared to that of unmodified BC or alginate strongly suggests high interpenetration between both polymers [22,24]. This hypothesis was also confirmed by the increase of the maximum thermal degradation temperature ($T_p$) caused by the presence of alginate in cellulose films, because the $T_p$ is considered a structural parameter related to the molecular weight, the crystallinity and the orientation of the polymers [28]. The intermediate of $T_p^{BC\text{-}Alg}$ value between those of both neat biopolymers indicates strong interaction between BC fibrils and Alg polymer chains (**Table I**).

DTGA analysis of the BC-Alg film showed a small third peak at 650ºC, similar to the peak observed for alginate in the range 700–750ºC. Besides, no peak was observed in the same range for the BC film samples **(Figure 1B)**. This result confirms the presence of alginate in the network of the BC film. Essentially, the thermogravimetric analysis of the BC-Alg scaffold clearly shows strong intermolecular interactions between BC and alginate in the hybrid film: the type of molecular interactions will be analyzed in the following sections by diffraction (XRD) and spectroscopic techniques (ATR-FTIR)

The structural properties of bacterial cellulose films containing alginate were studied by XRD (**Figure 2)**. The XRD profiles of BC and BC-Alg show the characteristic Bragg's angles for both matrices at 2θ= 14.6º, 16.9º and 22.8º, which are indexed as (ī 1 0), (0 1 0) and (1 0 0) reflection planes, respectively. The results revealed the presence of type-1 cellulose crystals in BC films, as was previously reported [29]. The XRD spectra of BC and BC-Alg displayed similar profiles related to the peak positions and distributions; those results indicate that the addition of alginate to the bacterial culture during the synthesis of the film does not alter the crystalline structure of the bacterial cellulose, as previously reported [24]. However, the comparative analysis of both XRD spectra showed two major differences associated with the change in intensity of the (ī 1 0) peak of BC-Alg, which is at least 3 times lower than that of BC, and also, the (1 0 0) peak in BC-Alg is wider than the same peak in BC. The results suggest some changes in the preferential orientation of the (ī 1 0) and (1 0 0) planes, as previously reported in BC film supplemented with polyethylene glycol, carboxymethyl- and hydroxypropyl cellulose or by complete water removal [29,30]. The changes observed in the BC-Alg nanocomposite could be attributed to the interaction between the highly hydroxylated biopolymers through hydrogen bridges. The addition of Alg to *A. xylinum* cultures during the synthesis of BC performed in nonstatic cultures decreases the crystallinity index and the crystallite size of the cellulose nanocomposite, as shown by XRD analysis. Similarly, the presence of alginate reduces the crystallinity index on BC films by about 1.4 times, from 71.0% to 49.7% but with a homogenous surface structure, as seen by SEM. Particularly, the reduction of the crystallinity index is generally related to an increment in the amorphous phase of films concomitantly with the increased water absorption capacity. Drastic reduction of the crystallinity index, attributed to the addition of different exogenous molecules, such as Tween 80, urea, Calcofluor White ST, hydroxypropylmethyl and carboxymethyl celluloses White ST, to the fermentation culture affects the synthesis of the bacterial cellulose network, as has been previously reported in cultures of *Gluconacetobacter xylinum* [29]. Low BC crystallinity values modified *in situ* by the addition of 0.04% of alginate to stirred cultures of *G. xylinum* cultures were reported previously [24]. However, the XRD analysis is not conclusive since the SEM micrographs showed nonuniform BC-Alg film surfaces with clumps [24]. The SEM images indicate an inhomogeneous gel structure that can be attributed to the strategy developed for cellulose production because of stirred culture conditions. Similarly, short cellulose nanofibrils were detected in microbial cultures under stirred conditions [21]. Short fibrils increase the randomness structure of bacterial cellulose pellicles, reducing the strength and stability of the BC films. Meanwhile, the static microbial cultivation method showed long cellulose nanofibrils displaying more structured organization of the film at the air–media interface (**Figure 3**). Additionally, images of both BC and BC-Alg show homogenous surfaces but with different characteristics (**Figure 3**). The BC film surface showed a typical bacterial cellulose network composed of long and entangled cellulose nanofibrils [31]. On the other hand, the nanocomposite BC-Alg films were homogenous with a more closed network. The presence of alginate in static cultures allowed the formation of a strong cooperative

network between the biopolymers without clumps, contrary to what was previously reported [24]. Our results indicate that the reduction of crystallinity can only be attributed to the strong interconnection of the BC fibrils and alginate polymer chains (**Figure 3**). The main differences between both types of BC-Alg nanocomposite surfaces could be attributed to the bacterial cultivation method.

The BC film surface roughness was reflected by the standard variation of the gray values of the selected area (200×300 μm) from the SEM 1,000x micrograph images (**Figure 3 A1 and A2**). The increase of standard variation values is proportional to the roughness of the analyzed surface. The analysis of roughness shows a 23% increase in standard deviation for the BC-Alg nanocomposite that can be correlated with a highly porous structure of the film network (**Figure 1S, Supplementary material**). The comparative analysis of the means showed that BC-Alg (136.063) is higher than BC (114.560), indicating a more regular spatial structure alignment of the biopolymer chains on the nanocomposite film due to the presence of alginate. Also, this result indicates the formation of a strong cooperative network allowing a more regular structure with the alignment of both types of biopolymeric chains. At the same time, BC-Alg films displayed a wide range of gray values, certainly due to the formation of an entwined network between both biopolymers with similar structural and chemical characteristics (**Figure 1S, Supplementary material**).

Later, the potential interactions between BC and Alg in the nanocomposite were analyzed by FTIR (**Figure 2S, Supplementary material)**. The BC film showed peaks centered at 3348 $cm^{-1}$ and 2890 $cm^{-1}$ assigned to O-H and C-H stretching, respectively. Also, peaks centered at 1375 $cm^{-1}$ and 1033 $cm^{-1}$ were observed and assigned to C-H bending and the characteristic vibration for sugar rings, respectively [32]. On the other hand, pure alginate showed characteristic peaks centered at 1593 $cm^{-1}$ and 1406 $cm^{-1}$, which are commonly assumed to be asymmetric and symmetric –carboxylic (-COO) stretching bands, respectively [33]. However, those characteristic $\upsilon(\text{-COO})_{asym}$ and $\upsilon(\text{-COO})_{sym}$ vibration bands were displaced to 1597 and 1425 $cm^{-1}$ in BC-Alg hybrid films, respectively. Comparison of the -COO vibrations in the spectra showed displacements, especially for $\upsilon(\text{-COO})_{sym}$ where the band shifted 19 $cm^{-1}$. Additionally, the O-H and C-H stretchings undergo frequency displacement to red and blue values, respectively (**Table II)**. These results could indicate that the water bound to the BC film is at least partially replaced by the highly hydrophilic alginate in the coacervate scaffold. The observed band shifts in the BC-Alg spectrum could be attributed to the intermolecular hydrogen bonds based on the functional groups of alginate and cellulose, rich in carboxylate and hydroxyl groups, respectively [20, 24]. The main molecular interactions determined by FTIR between both biopolymers clearly suggest high compatibility and the formation of an interpenetrating network by a co-gelation mechanism, named Morris model I [29]. These results suggest that alginate plays a crucial role in the biophysical properties of the BC matrix. The presence of alginate in the BC network exposes more hydrophilic groups that could further increase the film hydrophilicity. The increase of hydrophilicity in the BC film is advantageous since it can be related to the drug loading rise of water-soluble molecules such as doxorubicin. Doxorubicin is a water-soluble

molecule, but its hydrophilicity depends on the environment pH value. It is a weak base, with a primary amine group with a pKa of 8.30 [34]. At neutral pH, Dox occurs predominantly in its zwitterionic form with positive charge for the amine group and negative charge for the carboxylic group [35].

The comparative Brunauer–Emmett–Teller (BET) analysis of the films showed an increase of the surface area by about 84% and the rise of pore volume by more than 200% from the BC to the BC-Alg scaffolds **(Table III)**. Also, the pore size determined by the Barrett–Joyner–Halenda (BJH) model showed significant differences between the hybrid and BC films. These changes, which are attributed to the presence of a cooperative network of the BC and alginate biopolymers, might contribute to the potentiality of the films for Dox entrapment [36,37].

Therefore, analyses of BC-Alg films by TGA, XRD, FTIR, and SEM showed an intimate contact between alginate and cellulose chains, which results in an increase of the BC amorphous film structure enhancing the film hydrophilicity. The homogenous characteristic of BC-Alg nanocomposite films is relevant and desirable for the development of drug delivery since the molecular release kinetics of the cargo can be predictable, modeled and scaled up.

**3.2. Doxorubicin encapsulation**

BC-Alg coacervate films were loaded with doxorubicin by an absorption mechanism. First, native cellulose and hybrid cellulose films were exposed to 3.7 µmols/ml Dox solution. Dox loading was about 3 times higher for the BC-Alg than for the BC film (**Table IS, Supplementary material**), attributed to the presence of alginate in the BC network.

The increase of surface area, pore volume and size of BC-Alg films compared to unmodified BC films (**Table III**) can be correlated with the increase of the drug-film surface interactions and drug diffusion from the bulk to the film and consequently, more doxorubicin could be adsorbed and entrapped in the hybrid scaffold [38]. In addition, FTIR showed a strong interaction between both polymers, BC and Alg, creating a high interpenetrating biopolymeric network that contributes to enhanced entrapment and loading capacity of hydrophilic drug molecules such as doxorubicin. On the other hand, the ionic interactions of the net negative charges of the carboxylate groups in alginate and the positive net charge in Dox molecules could be responsible for enhancing the loading capability in the nanocomposite film, as previously reported by our laboratory [19]. Besides, hydroxyl groups of cellulose fibers and alginate chains could interact with Dox molecules making hydrogen bonds and stabilizing the drug loading in the coacervate film.

In order to determine the drug loading capacity, BC-Alg films were placed in contact with different doxorubicin amounts ranging from 3.7 to 11.0 µmol/ml (**Figure 4)**. A Dox loading of about 10 µmol/gram of film was found using a drug starting solution containing 3.7 µmol/ml of the drug. However, the Dox loading capacity of the BC–Alg films increased linearly ($r^2$= 0.95) when the drug concentrations were higher than 3.7 µmol/ml. Particularly, six times more Dox was incorporated into the BC-Alg film when the initial drug solution contained 11.0 µmol/ml compared to the solution of 3.7

μmol/ml (6:1 ratio). This fact is advantageous since the Dox content in the gel film can be tailored based on the patient conditions and therapeutic requirements.

The low loading capacities for the first initial concentration were attributed only to Dox–matrix interactions. Besides, when the drug concentration increased, Dox-Dox interactions inside the matrix became relevant, with a phenomenon commonly described as π–π stacking taking place [13].

**3.3. Doxorubicin release studies**

BC-Alg films containing different amounts of Dox incubated in PBS buffer showed similar hyperbolic kinetic drug release profiles (**Figure 5**). After burst-size drug release in each case, the percentage of Dox release remains almost constant at least for 14 days, but the amount of released drug is not the same in each loading case (**Table IIS, Supplementary material)**.

Dox release from the films could be explained by the existence of different molecular interactions between the drug and the film matrix. At low Dox loading, the main interactions between the drug and the BC-Alg film could be attributed to ionic and weak electrostatic interactions, as previously reported [19]. Meanwhile, at high amount of drug loaded into the film, other interactions such as the π-π of the Dox aromatic ring become more relevant, modifying the drug release profile, similar to what was mentioned for the Dox encapsulation mechanism. Finally, a linear relation was found between Dox loading and release rates ($r^2$= 0.97), becoming an important parameter for potential personalized therapy **(Figure 6)**.

**3.4. Cell viability assays**

The cell viability in HT-29 human colorectal adenocarcinoma cell cultures was tested for periods of 24 and 48 h using the BC-Alg films loaded with 9.55 and 42.25 μmol Dox /g matrix, which release 76 μM and 169 μM of drug at 24 h, and 77 μM and 181 μM of drug after 48 h of incubation in PBS, respectively. Similarly, controls based on the direct exposure of cells to soluble free Dox in the range 100–200 μM were assayed under the same experimental conditions.

Optical and fluorescent microscopy images from the cell cultures after 48 h of incubation were taken for systems containing free Dox free (in solution) and Dox released from the BC-Alg films. The presence of Dox precipitates was found in both systems **(Figure 3S and 4S, Supplementary material)**. However, the Dox crystallite lengths and quantities in the free drug solution were longer and bigger than those released from the films. The reduced crystallite amount and size can be analyzed considering the effect of the polymer as nucleation agent of the drug and the steric hindrance produced by the interpenetrating structure of the BC-Alg film network **(Figure 3)**. Besides, there might be diffusional restrictions of Dox to the solution imposed by the film [39,40]. The spectrofluorimetric analysis of supernatants containing Dox released from BC-Alg films did not show any shift in maximum wavelengths, suggesting the absence of potential complex formation between Dox and polymers after drug release that could affect the drug antitumor activity (data not shown).

Studies of free Dox tests on cell viability showed very little cell death in the 100–200 μM range of drug concentrations after 24 h of exposure. However, about 75% of cell viability was observed in the presence of 100 and 150 μM free Dox, which decreased to 63% of viability for 200 μM free Dox after 48 h **(Table IV)**. Meanwhile, BC-Alg nanocomposite films without Dox payload did not produce any cell damage. This result is quite relevant, especially because the BC-Alg biocompatibility assures a nontoxic effect on this cell line. Subsequently, cell viability decreased to 59% and 53% in the presence of BC-Alg films loaded with 9.55 and 42.25 μmols Dox/g, respectively, after 24 h incubation. However, cell viability using BC-Alg films loaded with 9.55 Dox μmols/g was 55% at 48 h but without significant differences ($p < 0.5$) compared to that observed at 24 h. Meanwhile, cell viability decreased by 16% (from 53% at 24 h to 37% at 48 h) when the cells were incubated with the BC-Alg films containing 42.25 Dox μmol/g (**Table IV)**. Additionally, pictures of cell cultures in DMEM after 48 h of exposure to free Dox (100–200 μM) showed a dark red precipitate, suggesting the presence of insoluble Dox in the media, but on the contrary, no dark red precipitate was visible to the naked eye when Dox was entrapped in the BC-Alg nanocomposite (42.5 μM/g)

These results clearly indicate a high anticancer effect with Dox loaded into the BC-Alg films **(Table IV)** compared to the free drug. Consequently, the cytotoxic effect of Dox can be modulated by the BC-Alg formulation, drug loading quantities and release kinetic conditions.

## 4. Conclusions

In the present work, a bacterial nanocellulose scaffold was modified by the incorporation of alginate in static cultures by the *in situ* method, providing a homogeneous biomaterial matrix with novel structural properties and keeping the chemotherapeutic agent doxorubicin for long periods of time. The performed techniques (TGA, FTIR, SEM) confirmed the alginate and bacterial cellulose intimate interaction by weak electrostatic forces, allowing the formation of a strong cooperative network with homogeneous increase of the amorphous phase (verified by XRD). The enhancement of the amorphous phase led to the exposure of large amounts of hydrophilic groups from alginate within the biomaterial environment that might help to improve Dox absorption on the films. Besides, the increase of surface area and pore volume enhanced the capacity of the BC-Alg scaffolds for the entrapment of Dox molecules. Also, the encapsulation assays demonstrated high Dox load rates in comparison with the unmodified bacterial cellulose. The drug loading of the BC-Alg nanocomposite scaffolds allows having more than 70 Dox μmols per gram of film. Dox kinetic release profiles of the films, obtained with different drug payloads, suggested a linear relationship between the amount of drug retained in the matrix and the amount of drug released, giving relevant information about BC-Alg/Dox interactions. The ability to tailor doxorubicin payload and release may help to define personalized therapy for the specific requirements of each patient.

BC-Alg scaffolds were tested on the colorectal adenocarcinoma cell line. The HT-29 human colorectal adenocarcinoma cell was chosen because it is recognized as a relatively Dox-resistant

cancer cell line. Direct exposure of the cells to Dox for 24 h showed almost no cell damage, but after 48 h of exposure, the cell viability decreased to values of around 70%. By comparison, the cells exposed to BC-Alg films showed a significant increase in cell damage at both times. Dox concentrations were measured from the cell culture supernatants, and similar values to those of free Dox experiments were found. Moreover, optical images taken from the supernatants showed that Dox released from BC-Alg scaffolds was less prone to form crystallites and consequently precipitation, which might be responsible for the decrease in cell toxicity on free Dox assays and the increased toxicity of anthracycline to tumor cells.

In conclusion, the bacterial cellulose-alginate nanocomposite was successfully developed, showing improved properties in terms of interpenetrating biopolymeric network, scaffold homogeneity, and ability for sustained release of doxorubicin as an implantable device for cancer treatment.

*In vivo* studies against solid tumor models in animals with the BC-Alg nanocomposite containing Dox are the next step to determine the potentiality of the scaffold for future ~~biomedical applications in~~ anticancer local therapies.

**References**


[1] WHO Cancer, (n.d.). http://www.who.int/mediacentre/factsheets/fs297/en/ (accessed November 18, 2015).

[2] J.B. Wolinsky, Y.L. Colson, M.W. Grinstaff, Local drug delivery strategies for cancer treatment: Gels, nanoparticles, polymeric films, rods, and wafers, J. Control. Release. 159 (2012) 14–26. doi:10.1016/j.jconrel.2011.11.031.

[3] J. Xu, Q. Zhao, Y. Jin, L. Qiu, High loading of hydrophilic/hydrophobic doxorubicin into polyphosphazene polymersome for breast cancer therapy, Nanomedicine Nanotechnology, Biol. Med. 10 (2014) 349–358. doi:10.1016/j.nano.2013.08.004.

[4] N.A. Dallas, L. Xia, F. Fan, M.J. Gray, P. Gaur, G. Van Buren, et al., Chemoresistant colorectal cancer cells, the cancer stem cell phenotype, and increased sensitivity to insulin-like growth factor-I receptor inhibition, Cancer Res. 69 (2009) 1951–1957. doi:10.1158/0008-5472.CAN-08-2023.

[5] H. Gelderblom, J. Verweij, K. Nooter, A. Sparreboom, Cremophor EL: The drawbacks and advantages of vehicle selection for drug formulation, Eur. J. Cancer. 37 (2001) 1590–1598. doi:10.1016/S0959-8049(01)00171-X.

[6] C.F. Thorn, C. Oshiro, S. Marsh, T. Hernandez-Boussard, H. McLeod, T.E. Klein, R.B. Altman, Doxorubicin pathways:pharmacodynamics and adverse effects, Pharmacogenet Genomics. 21 (2012) 440–446. doi:10.1097/FPC.0b013e32833ffb56.Doxorubicin.

[7] M.A. Moses, H. Brem, R. Langer, Advancing the field of drug delivery: Taking aim at cancer, Cancer Cell. 4 (2003) 337–341. doi:10.1016/S1535-6108(03)00276-9.

[8] B. Chiu, J. Coburn, M. Pilichowska, C. Holcroft, F.P. Seib, A. Charest, et al., Surgery combined with controlled-release doxorubicin silk films as a treatment strategy in an orthotopic neuroblastoma mouse model, Br. J. Cancer. 111 (2014) 708–715. doi:10.1038/bjc.2014.324.

focal treatment of primary breast cancer, Adv. Funct. Mater. 23 (2013) 58–65. doi:10.1002/adfm.201201238.

[10] B.H.A. Rehm, Alginates: Biology and Applications, 2009. doi:10.1017/CBO9781107415324.004.

[11] G.R. Castro, R.R. Kamdar, B. Panilaitis, D.L. Kaplan, Triggered release of proteins from emulsan-alginate beads, J. Control. Release. 109 (2005) 149–157. doi:10.1016/j.jconrel.2005.09.042.

[12] C. Dini, G.A. Islan, P.J. de Urraza, G.R. Castro, Novel Biopolymer Matrices for Microencapsulation of Phages: Enhanced Protection Against Acidity and Protease Activity, Macromol. Biosci. 12 (2012) 1200–1208. doi:10.1002/mabi.201200109.

[13] G.A. Islan, I.P. De Verti, S.G. Marchetti, G.R. Castro, Studies of ciprofloxacin encapsulation on alginate/pectin matrixes and its relationship with biodisponibility, Appl. Biochem. Biotechnol. 167 (2012) 1408–1420. doi:10.1007/s12010-012-9610-2.

[14] M.M. Abeer, M.C.I. Mohd Amin, C. Martin, A review of bacterial cellulose-based drug delivery systems: Their biochemistry, current approaches and future prospects, J. Pharm. Pharmacol. 66 (2014) 1047–1061. doi:10.1111/jphp.12234.

[15] A. Bodin, H. Backdahl, H. Fink, L. Gustafsson, B. Risberg, P. Gatenholm, Influence of cultivation conditions on mechanical and morphological properties of bacterial cellulose tubes, Biotechnol. Bioeng. 97 (2007) 425–434. doi:10.1002/bit.

[16] C. for D.E. and Research, Guidances (Drugs) - Guidance for Industry: Pyrogen and Endotoxins Testing: Questions and Answers, (n.d.). http://www.fda.gov/Drugs/GuidanceComplianceRegulatoryInformation/Guidances/ucm314718.htm (accessed November 18, 2015).

[17] M.L. Cacicedo, K. Cesca, V.E. Bosio, L. Porto, G.R. Castro, Self-assembly of carrageenin–CaCO3 hybrid microparticles on bacterial cellulose films for doxorubicin sustained delivery, J. Appl. Biomed. 13 (2015) 239–248. doi:10.1016/j.jab.2015.03.004.

[18] N. Shah, M. Ul-Islam, W.A. Khattak, J.K. Park, Overview of bacterial cellulose composites: A

multipurpose advanced material, Carbohydr. Polym. 98 (2013) 1585–1598. doi:10.1016/j.carbpol.2013.08.018.

[19] V.E. Bosio, V. Machain, A.G. López, I.O.P. De Berti, S.G. Marchetti, M. Mechetti, G.R. Castro, Binding and encapsulation of doxorubicin on smart pectin hydrogels for oral delivery, Appl. Biochem. Biotechnol. 167 (2012) 1365–1376. doi:10.1007/s12010-012-9641-8.

[20] N. Chiaoprakobkij, N. Sanchavanakit, K. Subbalekha, P. Pavasant, M. Phisalaphong, Characterization and biocompatibility of bacterial cellulose/alginate composite sponges with human keratinocytes and gingival fibroblasts, Carbohydr. Polym. 85 (2011) 548–553. doi:10.1016/j.carbpol.2011.03.011.

[21] S. Kirdponpattara, A. Khamkeaw, N. Sanchavanakit, P. Pavasant, M. Phisalaphong, Structural modification and characterization of bacterial cellulose-alginate composite scaffolds for tissue engineering, Carbohydr. Polym. 132 (2015) 146–155. doi:10.1016/j.carbpol.2015.06.059.

[22] M. Park, D. Lee, J. Hyun, Nanocellulose-alginate hydrogel for cell encapsulation., Carbohydr. Polym. 116 (2015) 223–8. doi:10.1016/j.carbpol.2014.07.059.

[23] W. Shao, H. Liu, X. Liu, S. Wang, J. Wu, R. Zhang, et al., Development of silver sulfadiazine loaded bacterial cellulose/sodium alginate composite films with enhanced antibacterial property, Carbohydr. Polym. 132 (2015) 351–358. doi:10.1016/j.carbpol.2015.06.057.

[24] L.L. Zhou, D.P. Sun, L.Y. Hu, Y.W. Li, J.Z. Yang, Effect of addition of sodium alginate on bacterial cellulose production by Acetobacter xylinum., J. Ind. Microbiol. Biotechnol. 34 (2007) 483–9. doi:10.1007/s10295-007-0218-4.

[25] T. Okajima, N. Keiko, Z. Heping, N. Ling, T. Tanabe, T. Yasuda, et al., Sensitive colorimetric bioassays for insulin-like growth factor (IGF) stimulation of cell proliferation and glucose consumption: use in studies of IGF analogs, Endocrinology. 130 (1992) 2201–2212.

[26] I.E. Leon, V. Porro, A.L. Di Virgilio, L.G. Naso, P.A.M. Williams, M. Bollati-Fogolín, et al., Antiproliferative and apoptosis-inducing activity of an oxidovanadium(IV) complex with the flavonoid silibinin against osteosarcoma cells, J. Biol. Inorg. Chem. 19 (2014) 59–74. doi:10.1007/s00775-013-1061-x.

[27] D. Lourdin, L. Coignard, H. Bizot, P. Colonna, Influence of equilibrium relative humidity and plasticizer concentration on the water content and glass transition of starch materials, Polymer (Guildf). 38 (1997) 5401–5406. doi:10.1016/S0032-3861(97)00082-7.

[28] S. Ouajai, R.A. Shanks, Composition, structure and thermal degradation of hemp cellulose after chemical treatments, Polym. Degrad. Stab. 89 (2005) 327–335. doi:10.1016/j.polymdegradstab.2005.01.016.

[29] H.C. Huang, L.C. Chen, S. Bin Lin, H.H. Chen, Nano-biomaterials application: In situ modification of bacterial cellulose structure by adding HPMC during fermentation, Carbohydr. Polym. 83 (2011) 979–987. doi:10.1016/j.carbpol.2010.09.011.

[30] Z. Cai, J. Kim, Bacterial cellulose/poly(ethylene glycol) composite: Characterization and first evaluation of biocompatibility, Cellulose 17 (2010) 83–91. doi:10.1007/s10570-009-9362-5.

[31] M.H. Kwak, J.E. Kim, J. Go, E.K. Koh, S.H. Song, H.J. Son, et al., Bacterial cellulose membrane produced by *Acetobacter* sp. A10 for burn wound dressing applications, Carbohydr. Polym. 122 (2015) 387–398. doi:10.1016/j.carbpol.2014.10.049.

[32] M. Kacuráková, FTIR study of plant cell wall model compounds: pectic polysaccharides and hemicelluloses, Carbohydr. Polym. 43 (2000) 195–203. doi:10.1016/S0144-8617(00)00151-X.

[33] H. Daemi, M. Barikani, Synthesis and characterization of calcium alginate nanoparticles, sodium homopolymannuronate salt and its calcium nanoparticles, Sci. Iran. 19 (2012) 2023–2028. doi:10.1016/j.scient.2012.10.005.

[34] M. Gonçalves, P. Figueira, D. Maciel, J. Rodrigues, X. Shi, H. Tomás, et al., Antitumor efficacy of doxorubicin-loaded laponite/alginate hybrid hydrogels, Macromol. Biosci. 14 (2014) 110–120. doi:10.1002/mabi.201300241.

[35] B.P. Mahoney, N. Raghunand, B. Baggett, R.J. Gillies, Tumor acidity, ion trapping and chemotherapeutics, Biochem. Pharmacol. 66 (2003) 1207–1218. doi:10.1016/S0006-2952(03)00467-2.

[36] J.L. Arias, M.A. Ruiz, M. López-Viota, Á. V. Delgado, Poly(alkylcyanoacrylate) colloidal particles as vehicles for antitumour drug delivery: A comparative study, Colloids Surfaces B Biointerfaces. 62 (2008) 64–70. doi:10.1016/j.colsurfb.2007.09.018.

[37] Y. Zhu, J. Shi, Y. Li, H. Chen, W. Shen, X.-P. Dong, Hollow mesoporous spheres with cubic pore network as a potential carrier for drug storage and its *in vitro* release kinetics, J. Mater. Res. 20 (2004) 54–61. doi:10.1557/JMR.2005.0035.

[38] R.J. Ahern, J.P. Hanrahan, J.M. Tobin, K.B. Ryan, A.M. Crean, Comparison of fenofibrate-mesoporous silica drug-loading processes for enhanced drug delivery, Eur. J. Pharm. Sci. 50 (2013) 400–409. doi:10.1016/j.ejps.2013.08.026.

[39] R. A-sasutjarit, A. Sirivat, P. Vayumhasuwan, Viscoelastic properties of Carbopol 940 gels and their relationships to piroxicam diffusion coefficients in gel bases, Pharm. Res. 22 (2005) 2134–2140. doi:10.1007/s11095-005-8244-2.

[40] E. Trovatti, C.S.R. Freire, P.C. Pinto, I.F. Almeida, P. Costa, A.J.D. Silvestre, et al., Bacterial cellulose membranes applied in topical and transdermal delivery of lidocaine hydrochloride and ibuprofen: In vitro diffusion studies, Int. J. Pharm. 435 (2012) 83–87. doi:10.1016/j.ijpharm.2012.01.002.

# Figures

**Figure 1**. Thermogravimetic analysis of bacterial cellulose (—), bacterial cellulose-alginate nanocomposite (---) and alginate (····). (A) TGA and (B) DTGA curves

**A**

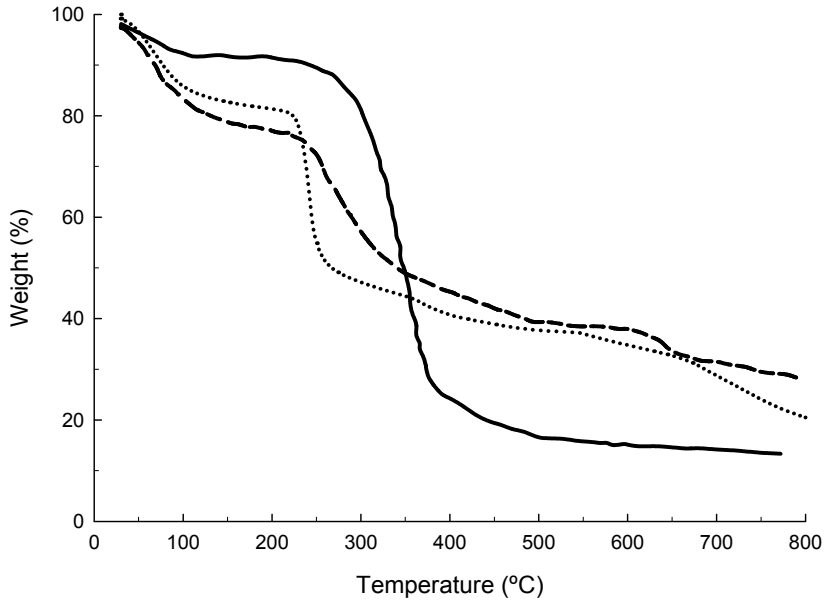


**B**

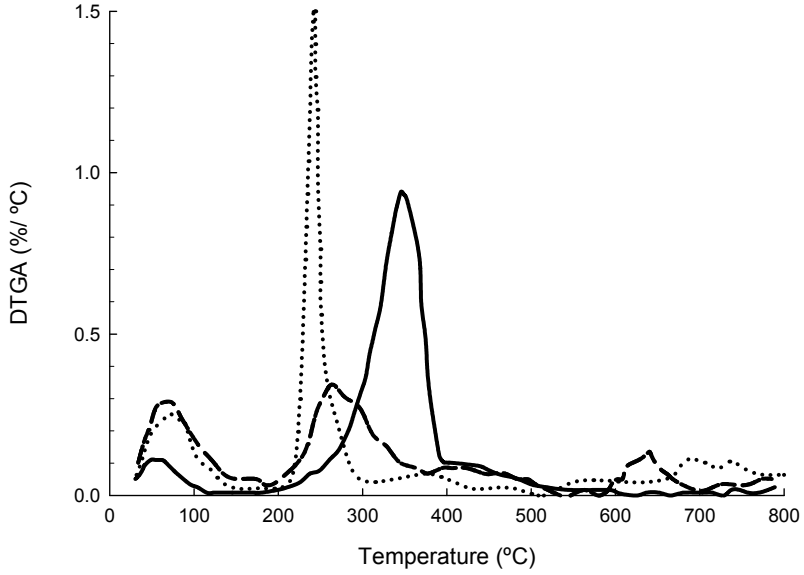

**Figure 2**. XRD spectra for bacterial cellulose (BC) and bacterial cellulose-alginate (BC-Alg) scaffolds.

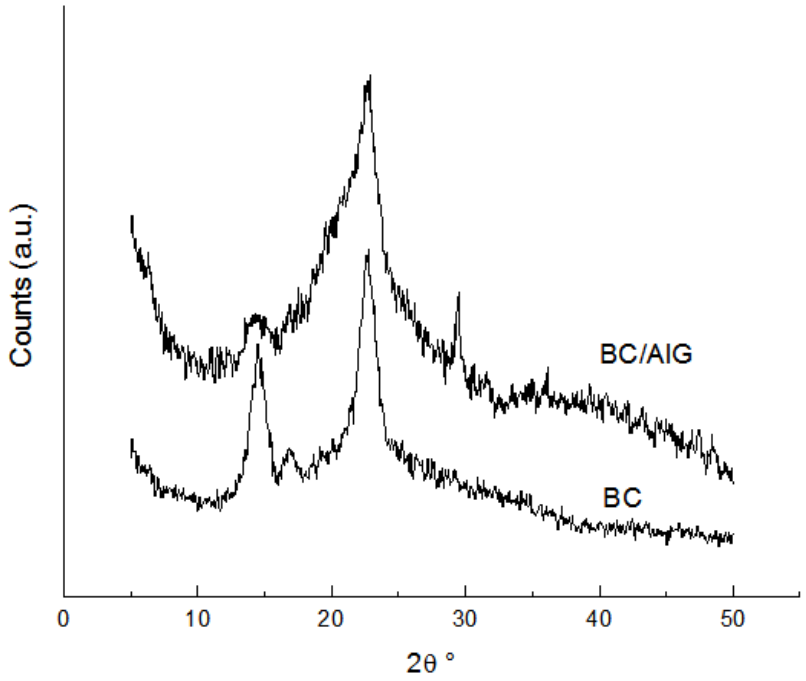

**Figure 3.** SEM images from BC scaffolds (A1, B1, C1) and from BC-Alg (A2, B2, C2). Letters: (A) 1,000X; (B) 5,000X; (C) 10,000X.

**A1**

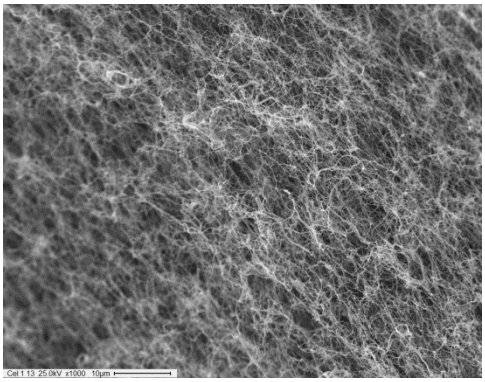

**A2**

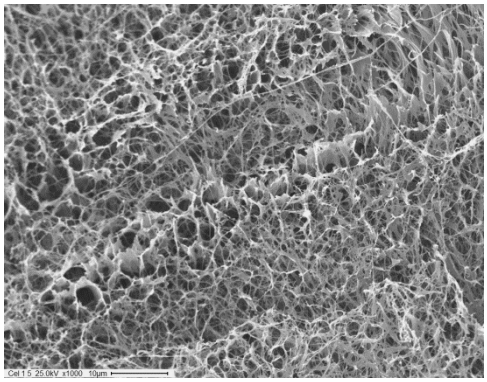

**B1**

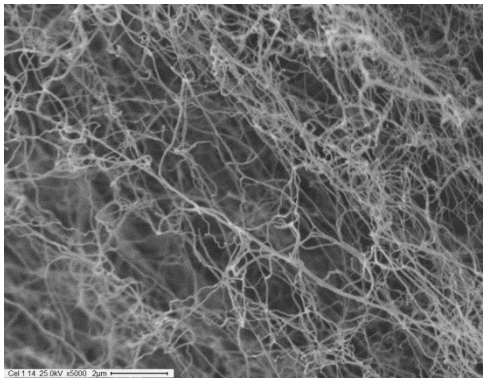

**B2**

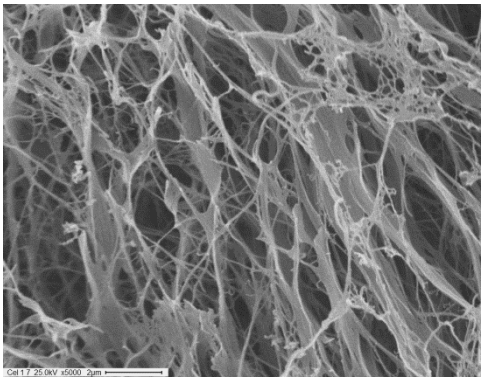

**C1**

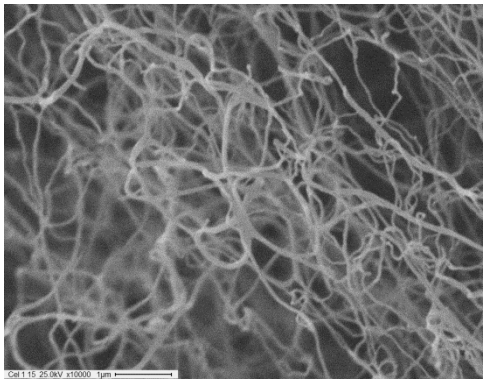

**C2**

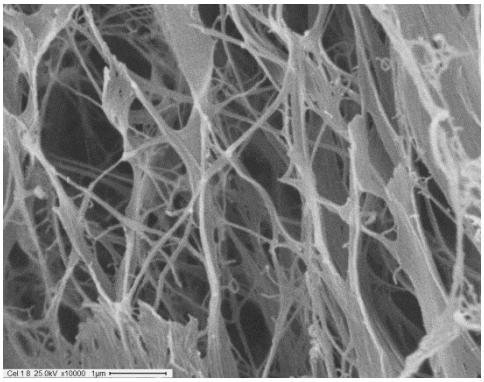

**Figure 4.** Entrapment of different starting doxorubicin concentrations in BC-Alg films after 20 h of incubation. Dox is expressed in μmol/gram of BC-Alg matrix. Errors bars represent the dispersion of the mean of at least three independent experiments.

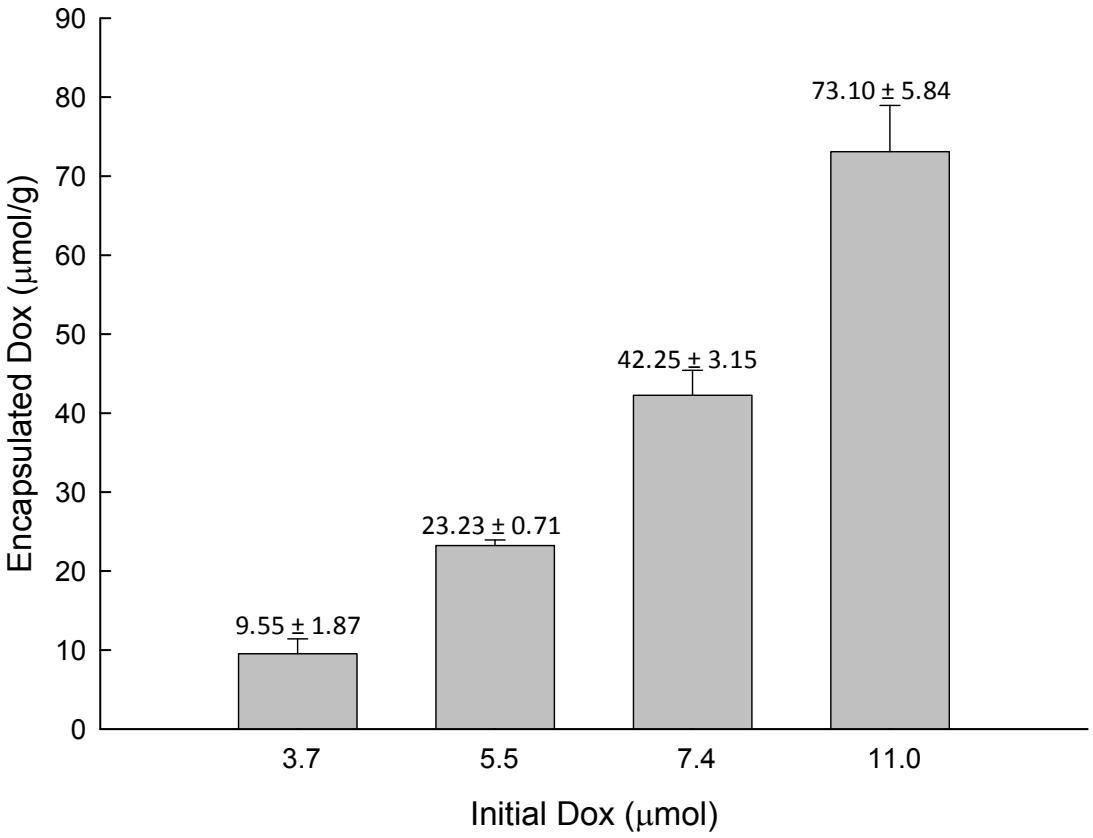

**Figure 5**. Doxorubicin release profiles from bacterial cellulose-alginate films loaded with different quantities of doxorubicin. Symbols of Dox initial loading amount: ○, 3.7 μmol; ▼, 5.5 μmol; △, 7.4 μmol and ■, 11.0 μmol. The values are the mean of three replicates (n = 3) with standard deviation (SD ⩽ 10%). Differences among the data were assessed for statistical significance by analysis of variance (ANOVA) with a significance level of 5.0% ($p < 0.05$).

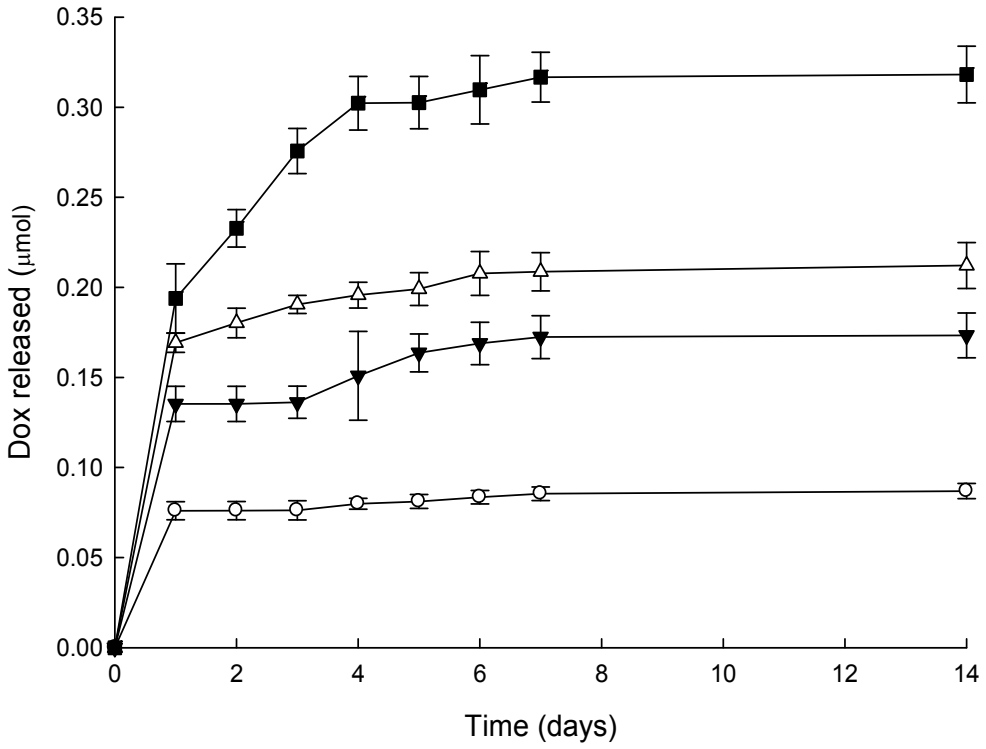

**Figure 6**. Relationship between Dox encapsulation rate and Dox released after 14 days under simulated physiologic conditions.

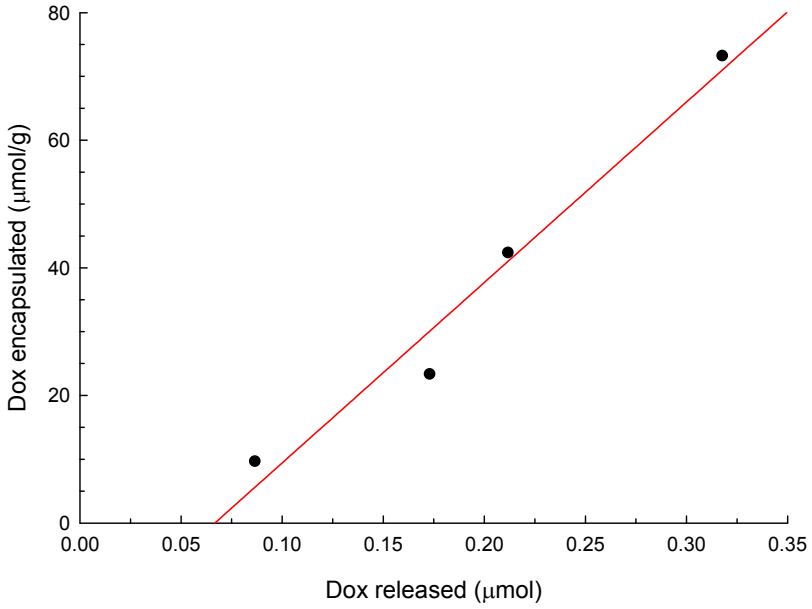

# Tables

**Table I.** Relevant values from thermal degradation analysis of native cellulose, hybrid cellulose and alginate scaffolds.

| Parameter | Films | | |
|---|---|---|---|
| | **Cellulose** | **Alginate** | **CB-Alg** |
| **Mass loss in 200-400°C range (%)** | 67.2 | 40.6 | 31.8 |
| **$T_p$ (°C)** | 345.6 | 243.0 | 265.3 |
| **Residue at 750°C (%)** | 13.5 | 24.1 | 29.5 |

**Table II**. FTIR analysis of bacterial cellulose, alginate and bacterial cellulose-alginate scaffolds.

| BC | Alginate | BC-Alg | Assignments |
|---|---|---|---|
| **(Wavenumbers, $cm^{-1}$)** | | | |
| 3348 | 3290 | 3342 | OH stretching |
| 2890 | 2929 | 2942 | C–H stretching |
| - | 1593 | 1597 | asymmetric –COO stretching |
| - | 1406 | 1425 | symmetric –COO stretching |
| 1375 | - | - | C–H bending |
| 1033 | 1026 | 1024 | C–O–C and C–O–H stretching vibration of sugar ring |

**Table III.** Adsorption and desorption analysis by BET of bacterial cellulose and bacterial cellulose-alginate films.

| **Matrix composition** | **Surface area ($m^2/g$)** | **Pore volume ($cm^3/g$)*** | **Pore size (nm)** | |
|---|---|---|---|---|
| | | | **BJH adsorption** | **BET method** |
| **BC** | 19.97 | 0.077 | 22.22 | 15.10 |
| **BC-Alg** | 36.76 | 0.23 | 27.95 | 22.11 |

***** BJH Adsorption cumulative volume of pores between 1.700 nm and 300.000 nm width.

In all cases standard deviation is lower than 5.0%.

**Table IV.** Viability assays of the HT-29 cell line from human colorectal adenocarcinoma exposed to soluble Dox concentrations and BC-Alg films loaded with Dox (9.55 and 42.25 μmol/g ) after 24 and 48 h of incubation. Mean ± s.e.m. of 3 independent experiments.

| System | Soluble Doxorubicin (μM) | Cell Viability (%) | |
|---|---|---|---|
| | | 24 hours | 48 hours |
| Free | 100 | 94.0 ± 3.7 | 74.0 ± 2.7 |
| | 150 | 93.0 ± 3.3 | 73.0 ± 2.7 |
| | 200 | 95.0 ± 2.7 | 63.0 ± 2.1 |

| | Encapsulated Dox (μmol/g) | Dox release (μM) | | Cell Viability (%) | |
|---|---|---|---|---|---|
| | | 24 hours | 48 hours | 24 hours | 48 hours |
| BC-Alg | - | - | - | 103.0 ± 3.1 | 97.4 ± 2.1 |
| | 9.55 ± 1.87 | 76.0 ± 5.0 | 169.0 ±5.0 | 59.0 ± 7.2 | 55.0 ± 8.2 |
| | 42.25 ± 3.15 | 77.0 ± 5.0 | 181.0 ± 8.0 | 53.0 ± 1.6 | 37.0 ± 0.5 |